NANO LETTERS

pubs.acs.org/NanoLett Letter

Electrically Actuated Varifocal Lens Based on Liquid-Crystal-Embedded Dielectric Metasurfaces

Melissa Bosch, Maxim R. Shcherbakov,* Kanghee Won, Hong-Seok Lee, Young Kim, and Gennady Shvets

Cite This: *Nano Lett.* 2021, 21, 3849−3856 Read Online

ACCESS | Metrics & More | Article Recommendations | Supporting Information

ABSTRACT: Compact varifocal lenses are essential to various imaging and vision technologies. However, existing varifocal elements typically rely on mechanically actuated systems with limited tuning speeds and scalability. Here, an ultrathin electrically controlled varifocal lens based on a liquid crystal (LC) encapsulated dielectric metasurface is demonstrated. Enabled by the field-dependent LC anisotropy, applying a voltage bias across the LC cell modifies the local phase response of the silicon meta-atoms, in turn modifying the metalens focal length. In a numerical implementation, a voltage-actuated metalens with continuous zoom and up to 20% total focal shift is demonstrated. The LC-based metalens concept is experimentally verified through the design and fabrication of a bifocal metalens that facilitates high-contrast switching between two discrete focal lengths upon application of a 9.8 V_{pp} voltage bias. Owing to their ultrathin thickness and adaptable design, LC-driven dielectric metasurfaces open new opportunities for compact varifocal lensing in a diversity of modern imaging applications.

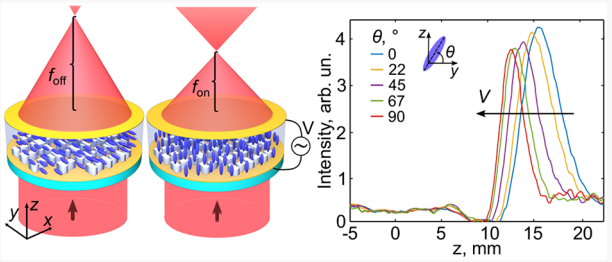

KEYWORDS: *Metalens, liquid crystals, tunable optics, design and optimization*

INTRODUCTION

Many optical systems rely on varifocal optical elements, which enable focusing at different planes of an imaged scene. Traditionally, optical zoom systems have consisted of moving lenses, an approach that requires large-footprint, mechanically complex solutions, and it remains an open challenge to realize miniature nonmechanically actuated varifocal optical elements. In the past decade, metasurfaces[1−3] emerged as a versatile and compact platform for light wavefront engineering and imaging. Metasurfaces enabled the next generation of flat optics:[2,4,5] polarizers,[6−8] efficient diffraction gratings,[9,10] holograms,[11−13] and lenses.[14−16] Metalenses[17] can deliver the functionalities of conventional convex or concave lenses within extremely thin form-factors by virtue of the engineered phase response of nanoscale plasmonic[18] or dielectric[19,20] resonators. However, the focal distance of a metalens is usually predetermined by nanofabrication, and special measures must be taken to enable varifocal functionalities. Varifocal metalenses have been shown by stretching the substrate,[21] changing the polarization of the incoming beam,[22] inhomogeneous heating,[23] and incorporating voltage-controlled elements.[24] Electrically actuated metalenses represent one of the most attractive varifocal devices with vast potentials for integration with existing head-up displays and lightweight cameras. Liquid crystals (LCs), ordered assemblies of highly anisotropic molecules, are ubiquitous in modern technology as highly efficient electrically actuated switching agents. Applying AC voltage across a liquid crystal cell (LCC) can change the alignment of LC molecules, enabling high-contrast refractive index tuning. Sensitivity of metasurface resonances to the refractive index of the surrounding medium has been used to show LC-enabled electrically and thermally switched resonances,[25−37] absorption,[38,39] beam deflection,[40−42] and aberrations,[43] as well as programmable spatial light modulation.[44,45] Such LC-metasurfaces enable optical tuning with LC cell thicknesses that are a fraction of those used by traditional LC-only modulators.[46,47] While electrically actuated ultrathin optics would advance the development of compact imaging systems, LC-based varifocal metalenses have remained elusive so far.

In this Letter, we demonstrate an ultrathin LC-based metalens whose focal length can be adjusted by voltage. We provide a generalized design approach for the constituent elements of the metalens, silicon-based meta-atoms, which have optimized phase responses for several intermediate orientations θ of the LC molecules. By generating a vast meta-atom library, imposing a set of appropriate constraints, and choosing optimized meta-atom candidates, we construct a

Received: January 26, 2021
Revised: April 20, 2021
Published: April 26, 2021

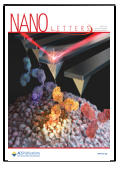

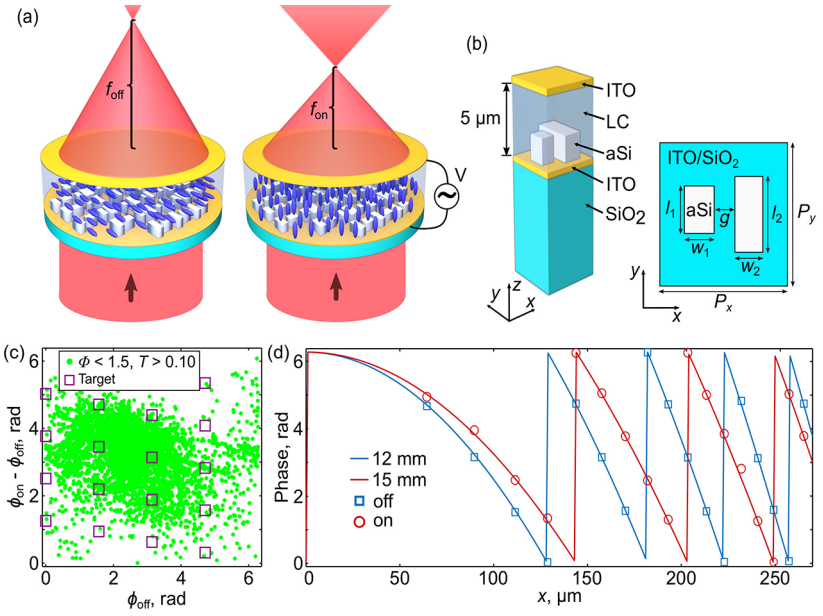

Figure 1. An ultrathin varifocal metalens encapsulated in electrically biased LCC. (a) The device and its operating principles: the focal length continuously varies from f_{off} (no bias) to f_{on} (V_0) (AC bias: $V = V_0 \cos 2\pi\nu t$). (b) Unit cell schematic: an array of amorphous silicon (aSi)-based meta-atoms encapsulated in an LCC is sandwiched between two biasing indium-tin-oxide (ITO) electrodes. (c) Green dots: meta-atom candidates selected from the five-dimensional parameter space ($l_{1,2}$, $w_{1,2}$, g) satisfying the phase-uniformity and transmittance criteria of $\Phi < 1.5$ (see eq 2) and $T > 0.10$. Purple squares: target values of ϕ_{on} and ϕ_{off} (four in each Fresnel zone). (d) The resulting phase distribution of the four-zone varifocal metalens in the "off" (blue squares) and "on" (red circles) states. Solid lines: the ideal phase functions of converging lenses with f_{off} = 15 mm and f_{on} = 12 mm. Other parameters include metasurface height of h = 300 nm and lattice periodicities of $P_x = P_y$ = 405 nm.

metalens that shows continuous focal distance shifting from f_{off} = 15 mm to f_{on} = 12 mm as a function of θ at a wavelength of λ = 690 nm. We extend the LC-driven metalens concept to conceive two wide-aperture bifocal lens with focal shifts as large as from f_{off} to $f_{on} = f_{off}/2$ and $f_{on} = -f_{off}$, respectively. We validate this concept by designing and fabricating a spherical bifocal metalens that emulates a transition between two distinct concave lenses. Energy redistribution between the f_{off} and $f_{on} = 2f_{off}$ focal spots manifests itself as intensity switching by up to 58% driven by low LCC voltages of <10 V_{pp}. Ultrathin LC-driven metalenses show flexible voltage-adjustable focal length control, appealing for use in compact and lightweight imaging devices.

RESULTS AND DISCUSSION

Varifocal Metalens Concept. The concept of the electrically actuated metalens is depicted in Figure 1a. It belongs to the family of Fresnel lenses, a concept that has been known and widely used since the early 19th century. Because of their inherently thin nature, Fresnel lenses have been installed (and are still found) atop lighthouses, where low-weight lenses are particularly attractive. A conventional lens focuses light at a focal distance of f using a continuously varying phase delay profile $\phi(r, f)$ given by[48]

$$\phi(r, f) = \frac{2\pi}{\lambda}(f - \sqrt{r^2 + f^2}) \quad (1)$$

where r is the radial distance from the lens center. Because a continuously varying phase delay requires that the lens thickness difference between its center and periphery exceeds the wavelength of light λ, Fresnel lenses overcome this limitation by dividing the lens into $m > 1$ Fresnel zones, each of which produces phase delay variations in the $0 < \phi_m < 2\pi$ ranges. The phase is "reset" at the beginning of each Fresnel zone.

A Fresnel-zone-plate metalens advances this idea further by discretizing each zone into n subzones with each subzone producing constant phase delays $0 < \phi_{m,n} < 2\pi/n$. Each subzone is comprised of an array of amorphous silicon (aSi) nanopillars, referred to as meta-atoms in the rest of this paper, encapsulated in a nematic LC. The design goal is to engineer the meta-atoms so as to impart a spatially varying phase delay profile $\phi_{m,n}$ onto the transmitted light, and to control $\phi_{m,n} \equiv \phi_{m,n}(\theta)$ using the rotation angle θ of the surrounding LC molecules. By varying the amplitude V_0 of an AC voltage $V = V_0 \cos 2\pi\nu t$ applied to the LCC, the LC orientation angle $\theta \equiv \theta(V_0)$ can be varied to ensure that the discretized phase delay $\phi_{m,n}(\theta)$ approximates $\phi(r, f(V_0))$ given by eq 1, where $f(V_0)$ is the voltage-dependent focal length. By varying bias voltage between its "off" ($V_0 = 0$) and "on" ($V_0 = V_{max}$) values, the focal distance $f_{on} < f(V_0) < f_{off}$ varies correspondingly.

A schematic of the aSi meta-atom, each comprised of two rectangular aSi pillars on an ITO-coated fused silica substrate, is shown in Figure 1b. Such meta-atom structures support localized electric and magnetic Mie-type resonant modes which may be excited by one of the principal linear polarizations of incident light and spectrally tuned by modifying the permittivity of the surrounding media. Dielectric metasurfaces with moderately high quality factors of the order $10 < Q < 100$ have been used for various applications, including polarization conversion and nonlinear optics.[8,49−51] The double-pillar meta-atom geometry shown in Figure 1b enables flexible control over the transmittance and the phase by varying the lengths $l_{1,2}$ and the widths $w_{1,2}$ of the pillars, as well as the gap g between them and the array periods P_x and P_y. The rest of the paper considers meta-atom responses for incident fields polarized along the y-axis.

https://doi.org/10.1021/acs.nanolett.1c00356
Nano Lett. 2021, 21, 3849−3856

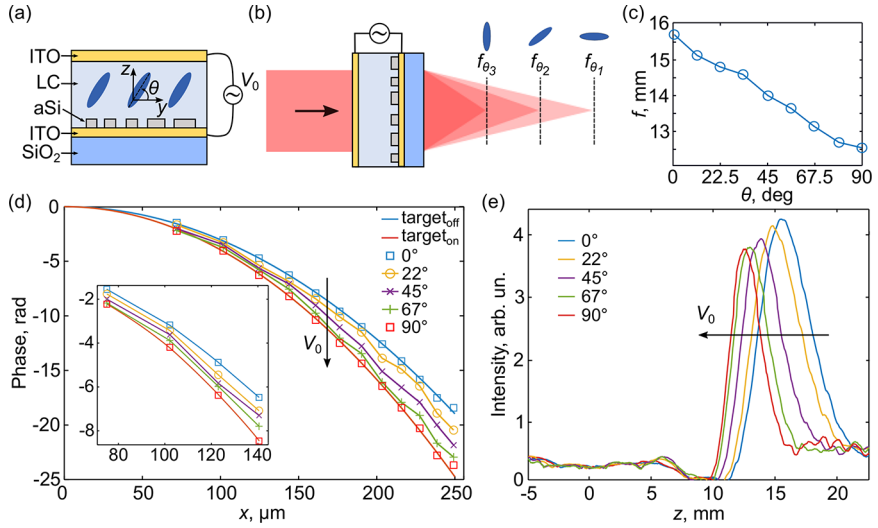

Figure 2. Liquid-crystal-driven metalens with a continuously tunable focal spot. (a) Schematic of the device. A silicon-based metalens is encapsulated in an LCC with a thickness of 5 μm between two transparent conducting oxide electrodes. An AC voltage is applied to the electrodes, driving the orientation of the LC molecules at angle θ with respect to the rubbing direction (y). (b) Applying voltage to the electrodes controls θ, continuously shifting the position of the focal spot. $\theta_{1,2,3}$ denote three representative LC angles with $\theta_1 < \theta_2 < \theta_3$, corresponding to three distinct focal spots. (c) Focal length of the lens as a function of θ. Solid line serves to guide the eye. (d) The phases of the scattered secondary waves by meta-atoms at positions x controlled by the LC in a cylindrical lens implementation. (e) On-axis intensity along the optical axis z for five values of θ.

The metasurface is covered by a 5 μm thick LC and ITO-coated fused silica top plate. The ITO layer renders the top and bottom glass plates conductive for use as electrodes that apply an AC bias across the LCC. The LC surrounding the metasurface can then be modeled as an anisotropic dielectric medium with $n_0 = 1.51$, $n_e = 1.72$, and V_0-dependent optical axis orientation angle θ (see Figure 2a for the definition of θ). In absence of an external voltage ($V_0 = 0$), the brushed top electrode induces a preferred in-plane anchoring direction of the LC along y across the whole LCC;[35] equivalently, here $\theta = 0°$. Applying a bias voltage with amplitude $V_0 > 0$ can increase θ up to a maximum value of 90°, therefore modifying the phase response of the meta-atom.

Adjusting the focusing profile of a metalens requires the phase modulation function to be tailored locally for each meta-atom. In order to fulfill this requirement, it is critical for the aSi meta-atom design space to permit both initial imparted phases ϕ_{off} and phase gradient $\Delta\phi \equiv \phi_{on} - \phi_{off}$ variations of the meta-atoms spanning the $0 < \Delta\phi < 2\pi$ range, while also maintaining acceptable transmittance T. We find this prerequisite is achieved for meta-atom thicknesses in the range $0.4\lambda < h < 1.5\lambda$, where λ is the targeted operation wavelength. Because fabricating meta-atom arrays of variable thickness using standard top-down methods is challenging, we select the same thickness $h \approx 0.4\lambda$ for all meta-atoms.

Design Principle. To approximate $\phi(r, f(\theta))$, we design a zone-plate metalens discretized into a series of concentric rings: Fresnel zones. Each ring (zone) corresponds to a 2π phase increment of the lens and is discretized by at least $n = 3$ meta-atom phase steps (subzones). To design an m-zone metalens with $f = f_{off}$ in the "off" state, n aSi meta-atoms per zone with varying geometric parameters are selected to impart phase shifts from $0 < \phi_{m,n}(\theta = 0°) < 2\pi$ in increments of $2\pi/n$ and are arranged to approximate the spatial phase profile according to $\phi_{m,n}(\theta = 0°) \approx \phi(r, f_{off})$. To enable electrical control over the focal length, the same procedure is followed in choosing the $N = n^*m$ total meta-atoms to simultaneously approximate the desired phase profile according to $\phi_{m,n}(\theta = 90°) \approx \phi(r, f_{on})$ for a, LC molecule orientation of $\theta = 90°$, corresponding to $V_0 = V_{max}$.

This selection enables a discrete bifocal lens switch, where tuning the LC molecule orientation from 0° to 90° switches the focal distance of the metalens from f_{off} to f_{on}. While discrete switching operation may be attractive in a variety of applications,[52,53] a truly varifocal metalens design is contingent on the meta-atoms satisfying two additional criteria at the intermediate LC molecule rotation angles $0° < \theta < 90°$.

Using numerical simulations, we found that imposing these two criteria over five discrete values of $\theta = 0°$, 22°, 45°, 67°, and 90° provides a good balance between the density of the candidate library and the quality of the varifocal operation. First, the phase for each meta-atom is sought as a monotonic (decreasing, in our case $f_{off} > f_{on}$) function of θ. Therefore, the phases of the meta-atoms $\phi(\theta)$ at the five values of θ have been set to satisfy the following constraints: $\phi(90°) < \phi(67°) < \phi(45°) < \phi(22°) < \phi(0°)$. Second, we found that the uniformity of the spacing between the phases $\phi(\theta)$ on the segment of $\theta \in [0°,90°]$ is of paramount importance in obtaining a truly varifocal lens (see Supporting Information Section 2). In other words, the preferable design requires that $\phi(\theta)$ changes near-linearly with the LC orientation angle θ. For quantitative characterization, we introduce the uniformity parameter Φ defined as

$$\Phi = \sum_{i=1}^{3} \frac{|\Delta\Phi_{i+1}| - |\Delta\Phi_i|}{3} \tag{2}$$

where $\Delta\Phi_1 = \phi(90°) - \phi(67°)$, $\Delta\Phi_2 = \phi(67°) - \phi(45°)$, $\Delta\Phi_3 = \phi(45°) - \phi(22°)$, and $\Delta\Phi_4 = \phi(22°) - \phi(0°)$. We found that applying the constraint of $\Phi < 1$ rad is important to achieve the truly varifocal function of the metalens. These two conditions ensure the selection of meta-atoms that provide a continuous and uniformly tuned phase profile of the metalens with V_0.

https://doi.org/10.1021/acs.nanolett.1c00356
Nano Lett. 2021, 21, 3849−3856

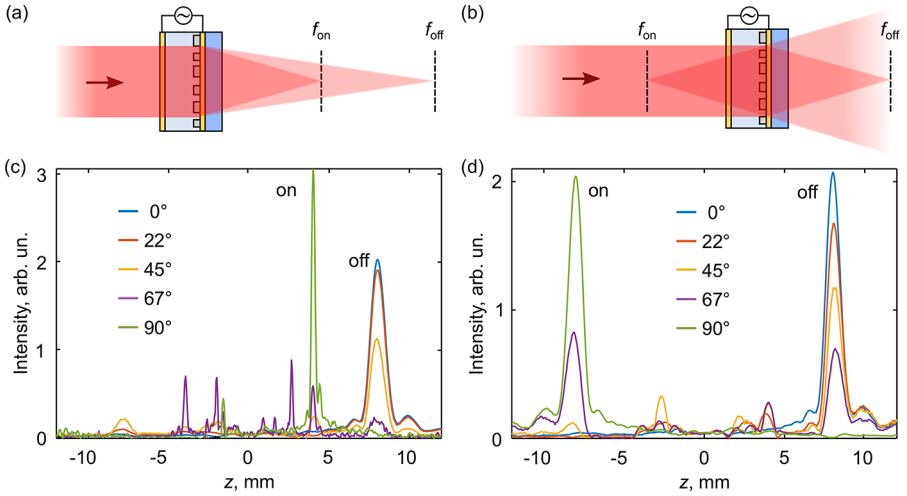

Figure 3. Simulation of a bifocal LC-controlled cylindrical metalens. (a) A sketch of Type I bifocal metalens: upon changing the orientation of the LC molecules from $\theta = 0°$ to $\theta = 90°$, the focal length of the metalens changes from f_{off} to $f_{on} = f_{off}/2$. (b) A sketch of Type II bifocal metalens: upon changing the orientation of the LC molecules from $\theta = 0°$ to $\theta = 90°$, the focal length of the metalens changes from f_{off} to $f_{on} = -f_{off}$. (c) Intensity along z showing focus at distances from $f_{off} = 8$ mm ($\theta = 0°$) to $f_{on} = 4$ mm ($\theta = 90°$) for a Type I bifocal metalens. (d) Intensity along z showing focusing at distances from $f_{off} = 8$ mm ($\theta = 0°$) to $f_{on} = -8$ mm ($\theta = 90°$) for a Type II bifocal metalens.

To illustrate the LC-encapsulated meta-atom optimization and selection process for a varifocal metalens, Figure 1c plots a map of simulated candidates which satisfy all of the imposed restrictions as a function of the two key phase quantities of a tunable lens, ϕ_{off} and $\Delta\Phi \equiv \phi_{on} - \phi_{off}$. Individual green points correspond to aSi unit cells with unique geometric parameters from a five-dimensional parameter space ($l_{1,2}$,$w_{1,2}$,g). The phase map covers almost the full $0-2\pi$ range along both axes, thereby permitting a wide range of f_{on} and f_{off} combinations. For example, squares on the map represent the targeted phase points for a lens with $f_{off} = 15$ mm, $f_{on} = 12$ mm, $n = 4$ subzones, and $m = 4$ Fresnel zones. The overlap between squares and green points in Figure 1c signifies the existence of at least one specific meta-atom candidate satisfying the metalens design. The selected candidates are plotted in Figure 1d as a function of x, arranged according to eq 1 and showing close agreement with the "off" and "on" targeted phase profiles.

Computational Design of a Varifocal Metalens. An LC-driven metalens with continuously tunable focal length is depicted in Figure 2a,b. Because of the voltage-induced realignment of the LC molecules to angles θ with respect to the "off" (y, see Figure 2a) direction, applying an AC voltage bias across the LCC continuously controls the focal spot position.

A three-zone ($m = 3$) metalens template with $\lambda = 690$ nm, $\Phi = 1$ rad, width of 500 μm, and focal distance targets $f_{off} = 12$ mm and $f_{on} = 15$ mm is designed to numerically demonstrate the focusing performance and varifocal tuning capability of an LC-driven metalens. We realize full-aperture simulations of the varifocal metalens by implementing the design as a cylindrical lens. The resulting simulated focal length of the metalens is plotted in Figure 2c as a function of $0° < \theta < 90°$. A smooth and near-constant rate of change of f with the LC angle is observed: $f^{-1}(\Delta f/\Delta\theta) \approx 0.22\%\cdot\text{deg}^{-1}$. The phase profile imparted onto transmitted light by the cylindrical metalens as a function of x is presented in Figure 2d for five values of θ. These results demonstrate a uniform and continuous phase modulation of 12 total subzones by modulating the LC orientation angle. The x-dependent phase imprinted by the metalens onto normally incident light starts near the targeted $\phi_{off}(r, f_{off} = 15$ mm) phase profile at $\theta = 0°$ ("off" orientation), and ends near the targeted $\phi_{on}(r, f_{on} = 12$ mm) phase profile at $\theta = 90°$ ("on" orientation). Remarkably, each of the five values of θ produces high-contrast focal spots along the optical axis of the lens (z) as depicted in Figure 2e. The focusing efficiency and Strehl ratio of the focal spots are calculated using well-established protocols[54,55] (see Supporting Information, Section 1).

The focusing efficiency of the metalens is found to be 12.1% for the "off" LC orientation and 13.6% for "on" LC orientation. The Strehl ratios of the device range between 0.72 to 0.83 for all LC angles, indicating near-diffraction-limited focusing performance.

Although $f_{off} = 15$ mm and $f_{on} = 12$ mm were the targets for our numerical demonstration, we note that the adaptability of our optimization approach enables the design of varifocal metalenses with nearly arbitrary focal length tuning ratios T, defined as $T = \frac{f_{off} - f_{on}}{f_{off}}$[56,57] (see Supporting Information Section 2).

Simplified Computational Design of Large Aperture Bifocal Metalenses. Several modern imaging technologies require tunable focus lenses with large apertures.[58] Scaling the metalens size can pose optimization challenges, since typically each 2π zone added to the lens requires n (one per subzone) unique meta-atom designs.

Here, we propose several types of LC-metalenses with judiciously selected focusing conditions for two discrete focal spots to bypass the aforementioned scaling limitations. Figure 3a,b presents two proposed types of bifocal LC-metalenses that can be scaled to large aperture sizes. For Type I, the focus changes from f_{off} to $f_{on} = f_{off}/2$, and for Type II the focus changes from f_{off} to $f_{on} = -f_{off}$ upon changing the orientation of the LC molecules from $\theta = 0°$ to $\theta = 90°$. The reduced functionality of the bifocal metalens enables a simplified metalens design with just three ($n = 3$) types of engineered meta-atoms. Nevertheless, this small number of designer meta-atoms is sufficient for creating high-performance LC-tunable bifocal metalenses with appreciable NA (>0.3).

https://doi.org/10.1021/acs.nanolett.1c00356
Nano Lett. 2021, 21, 3849−3856

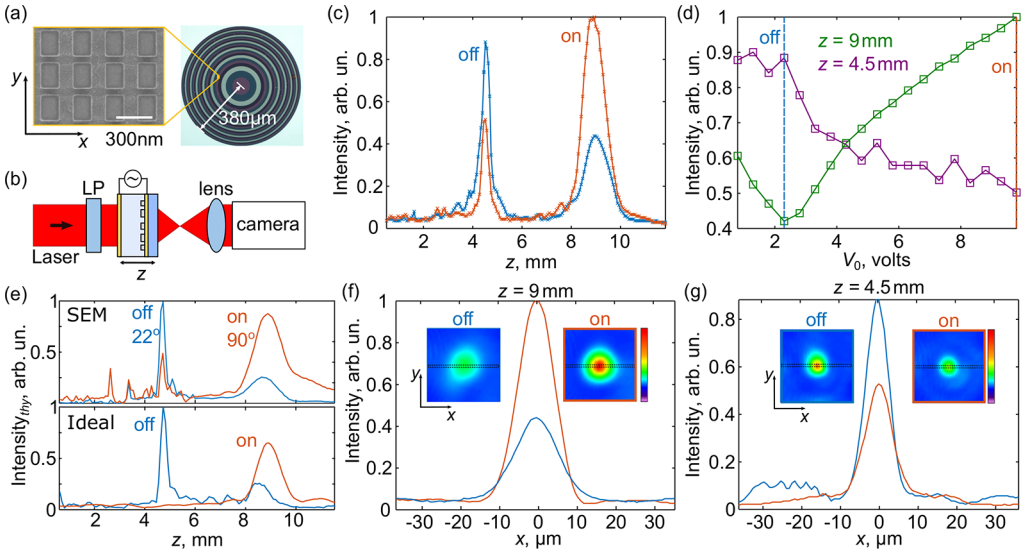

Figure 4. Experimental realization of an LC-controlled spherical bifocal metalens. (a) Left: A SEM image of the first metalens subzone. Right: Optical microscope image of the fabricated spherical metalens. The different shades of the metalens correspond to its four subzones. (b) Schematic of the measurement setup. LP is a linear polarizer. (c) A z-coordinate scan of the on-axis intensity for "off" (blue data points) and "on" (orange data points) states. Focal points at z = 9 mm and z = 4.5 mm are seen to exchange intensity as the voltage is changed between $V_0 = 2.2V_{pp}$ and $V_0 = 9.8V_{pp}$. (d) The focal spot intensities at $z = f_{on}$ and $z = f_{off}$ are plotted as a function of V_0. The dotted line indicates the "off" voltage, $V_0 = 2.2V_{pp}$. (e) Simulated intensity along the z-axis for (top) an SEM-based metalens design and (bottom) the ideal metalens design. (f) The x-sections of the z = 9 mm focal line image at $V_0 = 2.2V_{pp}$ and $V_0 = 9.8V_{pp}$. The insets show the respective camera images with the dashed rectangles denoting the y-averaging areas. (g) Same as (f) but for z = 4.5 mm.

Numerical demonstrations of wide-aperture LC-driven bifocal metalenses are accomplished for lens widths of 1 mm, λ_0 = 808 nm, n = 5, and f_{off} = 8 mm by applying the standard design routine and disregarding the additional varifocal constraints. The simulated intensity of light along the optical axis of the Type I and Type II cylindrical metalenses are plotted in Figure 3c,d, demonstrating high-contrast switching from f_{on} = 8 mm to f_{off} = 4 mm and f_{on} = 8 mm to $f_{off} = -8$ mm, respectively, when the LC alignment is changed from $\theta = 0°$ to $\theta = 90°$. The corresponding calculated focusing efficiencies of the Type I and Type II metalenses range between 22 and 27%. The Strehl ratios are above 0.8 for all "off" and "on" states, indicating diffraction-limited focusing capabilities of both devices.

Experimental Demonstration of an LC-Controlled Spherical Bifocal Metalens. The proof-of-concept experimental demonstration focuses on a Type I bifocal LC metalens design template consisting of single-pillar aSi meta-atoms, that is, $w_1 = w$, $l_2 = l$, $g = w_2 = l_2 = 0$, and $P_x = P_y \equiv P$. To ease fabrication complexity, it was necessary for the constituent meta-atoms of the metalens to have filling factors, defined as $F = wlP^{-2}$ in the range F = 0.15−0.45. Heuristically, the lateral geometry and bifocal phase constraints were concurrently achieved for a Type I template with n = 4 subzones, t = 300 nm, λ = 800 nm, and $f_{on} = 2f_{off}$ = 9 mm.

To experimentally verify the LC-driven metalens concept, a 760-μm-wide spherical metalens was fabricated on an ITO-coated SiO_2 substrate and encapsulated in a 5 μm-thick LC (see Supporting Information Sections 3 and 4). Figure 4a presents a scanning electron micrograph (SEM) of the first spherical metalens subzone and an optical microscope image of the metalens colored according to the four meta-atom geometries. The imaging setup depicted in Figure 4b and described in Supporting Information Section 6 was used to characterize the focusing and tuning performance of the samples. The results of this measurement are presented in Figure 4c, showing intensity maxima that occur at focal distances z = 9 mm and z = 4.5 mm for "off" and "on" voltages of $V_0 = 2.2\ V_{pp}$ and $V_0 = 9.8\ V_{pp}$, respectively. The focal spot intensities at $z = f$ and $z = f/2$ are plotted as a function of voltage in Figure 4d, demonstrating that the intensities of both focal spots behave as monotonic functions of voltage for $2.2\ V_{pp} < V_0 < 9.8\ V_{pp}$. The monotonic behavior is expected for the Type I bifocal design, as shown by the z-coordinate scan of the simulated on-axis intensity of the ideal metalens design (Figure 4e bottom panel). To more-closely model the experiment, the on-axis intensity as a function of z was simulated for a "realistic" metalens using geometrical parameters of the fabricated metalens and experimental laser wavelength (see Supporting Information Section 7). The results of this calculation are presented in the top panel of Figure 4e, showing excellent qualitative and quantitative agreement with the experimental results. An additional factor contributing to the discrepancies between the experiment and calculations could be the misalignment of the initial LC anchoring direction, a known issue of LC-metadevice fabrication.[59] Although it is not contained in our model, several strategies have recently emerged to mitigate LC alignment inhomogeneity and address its numerical modeling.[59−61] Figure 4f,g presents the measured voltage-dependent intensity line-cuts of the focal spots and 2D focal spot profiles of the metalens. By increasing the voltage from $V_0 = 2.2V_{pp}$ to $V_0 = 9.8V_{pp}$, the focal spot intensity at $z = f$ (Figure 4f) increases by 58%; for the same voltage increment, the focal spot intensity at $z = f/2$ (Figure 4g) decreases by 37%. The full width at half maximum of the f_{on} and f_{off} focal spots are 11.4 and 7.9 μm, respectively, comparable to that enabled by the diffraction limits 10.9 and 5.4 μm. The corresponding Strehl ratios of the "off" and "on" focal spots are 0.75 and 0.84, respectively (calculation details provided in Supporting Information Section 1).

https://doi.org/10.1021/acs.nanolett.1c00356
Nano Lett. 2021, 21, 3849−3856

Outlook and Conclusions. Although the operation wavelengths used in this work were 690 and 808 nm, the spectral range may be extended through appropriate meta-atom scaling and selection of constituent meta-atom materials with low Ohmic losses. For instance, GaP[62] and TiO_2[17,63] or crystalline Si[64,65] may enable high-performance LC-driven varifocal metalenses in the visible or infrared spectral ranges, respectively. Moreover, the experimental focusing efficiency is expected to increase with improved nanofabrication and LC alignment. Finally, by integrating our platform with recent technical advances in metasurfaces[19,20,66] we envision prospects for RGB operation and optical aberration correction to eventually find use in compact imagers, such as head-up displays and augmented reality glasses.

To conclude, we have demonstrated the electrostatic actuation of an LC-encapsulated dielectric metasurface for continuous and reversible varifocal lensing in the visible and near-IR spectral ranges. We present a metasurface design consisting of resonant aSi nanopillars encapsulated in a nematic LCC. A voltage bias applied across the cell tunes the resonance frequency of the aSi nanopillars, thereby enabling real-time control over the spatial phase profile imparted on the incident light and the resulting focal length of the metalens. Our numerical simulations have verified several metalens designs, including a metalens with the focal length tuning continuously from f = 12 mm to f = 15 mm, as well as metalenses with the focal length switchable between two discrete focal lengths. We experimentally demonstrate an LC-driven metalens which facilitates focal length switching between 9 mm and 4.5 mm when a low voltage bias of 9.8 V_{pp} is applied across the LCC. Our results establish LC-driven resonant dielectric metasurfaces as a versatile platform for electrically actuated varifocal metalenses, suitable for various applications where compact and tunable focusing devices are sought.

■ ASSOCIATED CONTENT

Supporting Information

The Supporting Information is available free of charge at https://pubs.acs.org/doi/10.1021/acs.nanolett.1c00356.

Simulation of meta-atoms and metalenses; focusing efficiency and Strehl ratio calculations; device fabrication; metalens design parameters; optical measurement description; testing of cylindrical metalenses (PDF)

■ AUTHOR INFORMATION

Corresponding Author

Maxim R. Shcherbakov − *School of Applied and Engineering Physics, Cornell University, Ithaca, New York 14853, United States;* orcid.org/0000-0001-7198-5482; Email: mrs356@cornell.edu

Authors

Melissa Bosch − *Department of Physics, Cornell University, Ithaca, New York 14853, United States*

Kanghee Won − *Samsung Advanced Institute of Technology (SAIT), Samsung Electronics, Co. Ltd., Suwon-si, Gyeonggi-do 16678, Republic of Korea*

Hong-Seok Lee − *Samsung Advanced Institute of Technology (SAIT), Samsung Electronics, Co. Ltd., Suwon-si, Gyeonggi-do 16678, Republic of Korea;* orcid.org/0000-0002-3081-7666

Young Kim − *Samsung Advanced Institute of Technology (SAIT), Samsung Electronics, Co. Ltd., Suwon-si, Gyeonggi-do 16678, Republic of Korea*

Gennady Shvets − *School of Applied and Engineering Physics, Cornell University, Ithaca, New York 14853, United States*

Complete contact information is available at: https://pubs.acs.org/10.1021/acs.nanolett.1c00356

Notes

The authors declare no competing financial interest.

■ ACKNOWLEDGMENTS

The authors thank Dragomir Neshev and Maxim Gorkunov for stimulating discussions. This work was supported by Global Research Outreach program of Samsung Advanced Institute of Technology and, in part, by the Cornell Center for Materials Research with funding from the NSF MRSEC program (DMR-1719875). This work was performed in part at the Cornell NanoScale Science and Technology Facility (CNF), a member of the National Nanotechnology Coordinated Infrastructure (NNCI), which is supported by the National Science Foundation (Grant NNCI-2025233). M.B. is supported by the National Science Foundation Graduate Research Fellowship (Grant DGE-1650441). G.S. acknowledges the support by the Office of Naval Research (ONR) under the Award No. N00014-21-1-2056.

■ REFERENCES

(1) Kildishev, A. V.; Boltasseva, A.; Shalaev, V. M. Planar photonics with metasurfaces. *Science* **2013**, *339*, 1232009.

(2) Yu, N.; Capasso, F. Flat optics with designer metasurfaces. *Nat. Mater.* **2014**, *13*, 139−150.

(3) Kamali, S. M.; Arbabi, E.; Arbabi, A.; Faraon, A. A review of dielectric optical metasurfaces for wavefront control. *Nanophotonics* **2018**, *7*, 1041−1068.

(4) Lin, D.; Fan, P.; Hasman, E.; Brongersma, M. L. Dielectric gradient metasurface optical elements. *Science* **2014**, *345*, 298−302.

(5) Lawrence, M.; Barton, D. R.; Dixon, J.; Song, J. H.; van de Groep, J.; Brongersma, M. L.; Dionne, J. A. High quality factor phase gradient metasurfaces. *Nat. Nanotechnol.* **2020**, *15*, 956−961.

(6) Zhao, Y.; Alù, A. Manipulating light polarization with ultrathin plasmonic metasurfaces. *Phys. Rev. B: Condens. Matter Mater. Phys.* **2011**, *84*, 205428.

(7) Balthasar Mueller, J. P.; Rubin, N. A.; Devlin, R. C.; Groever, B.; Capasso, F. Metasurface polarization optics: Independent phase control of arbitrary orthogonal states of polarization. *Phys. Rev. Lett.* **2017**, *118*, 113901.

(8) Bosch, M.; Shcherbakov, M. R.; Fan, Z.; Shvets, G. Polarization states synthesizer based on a thermo-optic dielectric metasurface. *J. Appl. Phys.* **2019**, *126*, 073102.

(9) Ding, F.; Pors, A.; Bozhevolnyi, S. I. Gradient metasurfaces: A review of fundamentals and applications. *Rep. Prog. Phys.* **2018**, *81*, 026401.

(10) Fan, Z.; Shcherbakov, M. R.; Allen, M.; Allen, J.; Wenner, B.; Shvets, G. Perfect diffraction with multiresonant bianisotropic metagratings. *ACS Photonics* **2018**, *5*, 4303−4311.

(11) Ni, X.; Kildishev, A. V.; Shalaev, V. M. Metasurface holograms for visible light. *Nat. Commun.* **2013**, *4*, 2807.

(12) Zheng, G.; Mühlenbernd, H.; Kenney, M.; Li, G.; Zentgraf, T.; Zhang, S. Metasurface holograms reaching 80% efficiency. *Nat. Nanotechnol.* **2015**, *10*, 308−312.

(13) Wang, L.; Kruk, S.; Tang, H.; Li, T.; Kravchenko, I.; Neshev, D. N.; Kivshar, Y. S. Grayscale transparent metasurface holograms. *Optica* **2016**, *3*, 1504.

(14) Khorasaninejad, M.; Zhu, A. Y.; Roques-Carmes, C.; Chen, W. T.; Oh, J.; Mishra, I.; Devlin, R. C.; Capasso, F. Polarization-

insensitive metalenses at visible wavelengths. *Nano Lett.* **2016**, *16*, 7229−7234.
(15) Khorasaninejad, M.; Chen, W. T.; Devlin, R. C.; Oh, J.; Zhu, A. Y.; Capasso, F. Metalenses at visible wavelengths: Diffraction-limited focusing and subwavelength resolution imaging. *Science* **2016**, *352*, 1190−1194.
(16) Paniagua-Dominguez, R.; Yu, Y. F.; Khaidarov, E.; Choi, S.; Leong, V.; Bakker, R. M.; Liang, X.; Fu, Y. H.; Valuckas, V.; Krivitsky, L. A.; Kuznetsov, A. I. A metalens with a near-Unity numerical aperture. *Nano Lett.* **2018**, *18*, 2124−2132.
(17) Khorasaninejad, M.; Capasso, F. Metalenses: Versatile multifunctional photonic components. *Science* **2017**, *358*, eaam8100.
(18) Fu, Y.; Zhou, X. Plasmonic lenses: A review. *Plasmonics* **2010**, *5*, 287−310.
(19) Wang, S.; et al. A broadband achromatic metalens in the visible. *Nat. Nanotechnol.* **2018**, *13*, 227−232.
(20) Shrestha, S.; Overvig, A. C.; Lu, M.; Stein, A.; Yu, N. Broadband achromatic dielectric metalenses. *Light: Sci. Appl.* **2018**, *7*, 85.
(21) Kamali, S. M.; Arbabi, E.; Arbabi, A.; Horie, Y.; Faraon, A. Highly tunable elastic dielectric metasurface lenses. *Laser and Photonics Reviews* **2016**, *10*, 1002−1008.
(22) Zhou, S.; Shen, Z.; Li, X.; Ge, S.; Lu, Y.; Hu, W. Liquid crystal integrated metalens with dynamic focusing property. *Opt. Lett.* **2020**, *45*, 4324.
(23) Afridi, A.; Canet-Ferrer, J.; Philippet, L.; Osmond, J.; Berto, P.; Quidant, R. Electrically driven varifocal silicon metalens. *ACS Photonics* **2018**, *5*, 4497−4503.
(24) Chen, K.; Feng, Y.; Monticone, F.; Zhao, J.; Zhu, B.; Jiang, T.; Zhang, L.; Kim, Y.; Ding, X.; Zhang, S.; Alu, A.; Qiu, C.-W. A reconfigurable active Huygens' metalens. *Adv. Mater.* **2017**, *29*, 1606422.
(25) Müller, J.; Sönnichsen, C.; von Poschinger, H.; von Plessen, G.; Klar, T. A.; Feldmann, J. Electrically controlled light scattering with single metal nanoparticles. *Appl. Phys. Lett.* **2002**, *81*, 171−173.
(26) Kossyrev, P. A.; Yin, A.; Cloutier, S. G.; Cardimona, D. A.; Huang, D.; Alsing, P. M.; Xu, J. M. Electric field tuning of plasmonic response of nanodot array in liquid crystal matrix. *Nano Lett.* **2005**, *5*, 1978−1981.
(27) Gorkunov, M. V.; Osipov, M. A. Tunability of wire-grid metamaterial immersed into nematic liquid crystal. *J. Appl. Phys.* **2008**, *103*, 036101.
(28) Xiao, S.; Chettiar, U. K.; Kildishev, A. V.; Drachev, V.; Khoo, I. C.; Shalaev, V. M. Tunable magnetic response of metamaterials. *Appl. Phys. Lett.* **2009**, *95*, 033115.
(29) Kang, B.; Woo, J. H.; Choi, E.; Lee, H.-H.; Kim, E. S.; Kim, J.; Hwang, T.-J.; Park, Y.-S.; Kim, D. H.; Wu, J. W. Optical switching of near infrared light transmission in metamaterial-liquid crystal cell structure. *Opt. Express* **2010**, *18*, 16492.
(30) Decker, M.; Kremers, C.; Minovich, A.; Staude, I.; Miroshnichenko, A. E.; Chigrin, D.; Neshev, D. N.; Jagadish, C.; Kivshar, Y. S. Electro-optical switching by liquid-crystal controlled metasurfaces. *Opt. Express* **2013**, *21*, 8879.
(31) Buchnev, O.; Ou, J. Y.; Kaczmarek, M.; Zheludev, N. I.; Fedotov, V. A. Electro-optical control in a plasmonic metamaterial hybridised with a liquid-crystal cell. *Opt. Express* **2013**, *21*, 1633.
(32) Atorf, B.; Mühlenbernd, H.; Muldarisnur, M.; Zentgraf, T.; Kitzerow, H. Electro-optic tuning of split ring resonators embedded in a liquid crystal. *Opt. Lett.* **2014**, *39*, 1129.
(33) Sautter, J.; Staude, I.; Decker, M.; Rusak, E.; Neshev, D. N.; Brener, I.; Kivshar, Y. S. Active tuning of all-dielectric metasurfaces. *ACS Nano* **2015**, *9*, 4308−4315.
(34) Buchnev, O.; Podoliak, N.; Kaczmarek, M.; Zheludev, N. I.; Fedotov, V. A. Electrically controlled nanostructured metasurface loaded with liquid crystal: toward multifunctional photonic switch. *Adv. Opt. Mater.* **2015**, *3*, 674−679.
(35) Komar, A.; Fang, Z.; Bohn, J.; Sautter, J.; Decker, M.; Miroshnichenko, A.; Pertsch, T.; Brener, I.; Kivshar, Y. S.; Staude, I.; Neshev, D. N. Electrically tunable all-dielectric optical metasurfaces based on liquid crystals. *Appl. Phys. Lett.* **2017**, *110*, 071109.
(36) Parry, M.; Komar, A.; Hopkins, B.; Campione, S.; Liu, S.; Miroshnichenko, A. E.; Nogan, J.; Sinclair, M. B.; Brener, I.; Neshev, D. N. Active tuning of high-Q dielectric metasurfaces. *Appl. Phys. Lett.* **2017**, *111*, 053102.
(37) Xie, Z.-W.; Yang, J.-H.; Vashistha, V.; Lee, W.; Chen, K.-P. Liquid-crystal tunable color filters based on aluminum metasurfaces. *Opt. Express* **2017**, *25*, 30764.
(38) Shrekenhamer, D.; Chen, W. C.; Padilla, W. J. Liquid crystal tunable metamaterial absorber. *Phys. Rev. Lett.* **2013**, *110*, 177403.
(39) Wang, L.; Ge, S.; Hu, W.; Nakajima, M.; Lu, Y. Graphene-assisted high-efficiency liquid crystal tunable terahertz metamaterial absorber. *Opt. Express* **2017**, *25*, 23873.
(40) Komar, A.; Paniagua-Domínguez, R.; Miroshnichenko, A.; Yu, Y. F.; Kivshar, Y. S.; Kuznetsov, A. I.; Neshev, D. Dynamic beam switching by liquid crystal tunable dielectric metasurfaces. *ACS Photonics* **2018**, *5*, 1742−1748.
(41) Chung, H.; Miller, O. D. Tunable metasurface inverse design for 80% switching efficiencies and 144° angular deflection. *ACS Photonics* **2020**, *7*, 2236−2243.
(42) Gorkunov, M. V.; Kasyanova, I. V.; Artemov, V. V.; Ezhov, A. A.; Mamonova, A. V.; Simdyankin, I. V.; Palto, S. P. Superperiodic liquid-crystal metasurfaces for electrically controlled anomalous refraction. *ACS Photonics* **2020**, *7*, 3096−3105.
(43) Shen, Z.; Zhou, S.; Li, X.; Ge, S.; Chen, P.; Hu, W.; Lu, Y. Liquid crystal integrated metalens with tunable chromatic aberration. *Advanced Photonics* **2020**, *2*, 036002.
(44) Li, S.-Q.; Xu, X.; Maruthiyodan Veetil, R.; Valuckas, V.; Paniagua-Dominguez, R.; Kuznetsov, A. I. Phase-only transmissive spatial light modulator based on tunable dielectric metasurface. *Science* **2019**, *364*, 1087−1090.
(45) Wu, J.; Shen, Z.; Ge, S.; Chen, B.; Shen, Z.; Wang, T.; Zhang, C.; Hu, W.; Fan, K.; Padilla, W.; Lu, Y.; Jin, B.; Chen, J.; Wu, P. Liquid crystal programmable metasurface for terahertz beam steering. *Appl. Phys. Lett.* **2020**, *116*, 131104.
(46) Algorri, J.; Morawiak, P.; Bennis, N.; Zografopoulos, D.; Urruchi, V.; Rodríguez-Cobo, L.; Jaroszewicz, L. R.; Sánchez-Pena, J.; López-Higuera, J. M. Positive-negative tunable liquid crystal lenses based on a microstructured transmission line. *Sci. Rep.* **2020**, *10*, 10153.
(47) Li, L.; Bryant, D.; van Heugten, T.; Bos, P. J. Physical limitations and fundamental factors affecting performance of liquid crystal tunable lenses with concentric electrode rings. *Appl. Opt.* **2013**, *52*, 1978−1986.
(48) Goodman, J. W. *Introduction to Fourier optics*; Roberts and Company Publishers, 2005.
(49) Wu, C.; Arju, N.; Kelp, G.; Fan, J. A.; Dominguez, J.; Gonzales, E.; Tutuc, E.; Brener, I.; Shvets, G. Spectrally selective chiral silicon metasurfaces based on infrared Fano resonances. *Nat. Commun.* **2014**, *5*, 3892.
(50) Neuner, B., III; Wu, C.; Eyck, G. T.; Sinclair, M.; Brener, I.; Shvets, G. Efficient infrared thermal emitters based on low-albedo polaritonic meta-surfaces. *Appl. Phys. Lett.* **2013**, *102*, 211111.
(51) Shcherbakov, M. R.; Werner, K.; Fan, Z.; Talisa, N.; Chowdhury, E.; Shvets, G. Photon acceleration and tunable broadband harmonics generation in nonlinear time-dependent metasurfaces. *Nat. Commun.* **2019**, *10*, 1345.
(52) Love, G. D.; Hoffman, D. M.; Hands, P. J.; Gao, J.; Kirby, A. K.; Banks, M. S. High-speed switchable lens enables the development of a volumetric stereoscopic display. *Opt. Express* **2009**, *17*, 15716.
(53) Li, G.; Mathine, D. L.; Valley, P.; Äyräs, P.; Haddock, J. N.; Giridhar, M. S.; Williby, G.; Schwiegerling, J.; Meredith, G. R.; Kippelen, B.; Honkanen, S.; Peyghambarian, N. Switchable electro-optic diffractive lens with high efficiency for ophthalmic applications. *Proc. Natl. Acad. Sci. U. S. A.* **2006**, *103*, 6100−6104.
(54) Arbabi, A.; Horie, Y.; Ball, A. J.; Bagheri, M.; Faraon, A. Subwavelength-thick lenses with high numerical apertures and large

https://doi.org/10.1021/acs.nanolett.1c00356
Nano Lett. 2021, 21, 3849−3856

efficiency based on high-contrast transmitarrays. *Nat. Commun.* **2015**, *6*, 7069.
(55) Khorasaninejad, M.; Chen, W. T.; Zhu, A. Y.; Oh, J.; Devlin, R. C.; Roques-Carmes, C.; Mishra, I.; Capasso, F. Visible wavelength planar metalenses based on titanium dioxide. *IEEE J. Sel. Top. Quantum Electron.* **2017**, *23*, 43−58.
(56) Cheng, C.-C.; Alex Chang, C.; Andrew Yeh, J. Variable focus dielectric liquid droplet lens. *Opt. Express* **2006**, *14*, 4101−4106.
(57) Tseng, M. L.; Hsiao, H.-H.; Chu, C. H.; Chen, M. K.; Sun, G.; Liu, A.-Q.; Tsai, D. P. Metalenses: advances and applications. *Adv. Opt. Mater.* **2018**, *6*, 1800554.
(58) Hong, C.; Colburn, S.; Majumdar, A. Flat metaform near-eye visor. *Appl. Opt.* **2017**, *56*, 8822−8827.
(59) Sun, M.; Xu, X.; Sun, X. W.; Liang, X.'a.; Valuckas, V.; Zheng, Y.; Paniagua-Dominguez, R.; Kuznetsov, A. I.; et al. Efficient visible light modulation based on electrically tunable all dielectric metasurfaces embedded in thin-layer nematic liquid crystals. *Sci. Rep.* **2019**, *9*, 8673.
(60) Dolan, J. A.; Cai, H.; Delalande, L.; Li, X.; Martinson, A. B.; de Pablo, J. J.; López, D.; Nealey, P. F. Broadband liquid crystal tunable metasurfaces in the visible: Liquid crystal inhomogeneities across the metasurface parameter space. *ACS Photonics* **2021**, *8*, 567−575.
(61) Lininger, A.; Zhu, A. Y.; Park, J.-S.; Palermo, G.; Chatterjee, S.; Boyd, J.; Capasso, F.; Strangi, G. Optical properties of metasurfaces infiltrated with liquid crystals. *Proc. Natl. Acad. Sci. U. S. A.* **2020**, *117*, 20390−20396.
(62) Cambiasso, J.; Grinblat, G.; Li, Y.; Rakovich, A.; Cortés, E.; Maier, S. A. Bridging the gap between dielectric nanophotonics and the visible regime with effectively lossless gallium phosphide antennas. *Nano Lett.* **2017**, *17*, 1219−1225.
(63) Devlin, R. C.; Khorasaninejad, M.; Chen, W. T.; Oh, J.; Capasso, F. Broadband high-efficiency dielectric metasurfaces for the visible spectrum. *Proc. Natl. Acad. Sci. U. S. A.* **2016**, *113*, 10473−10478.
(64) Miller, S. A.; Yu, M.; Ji, X.; Griffith, A. G.; Cardenas, J.; Gaeta, A. L.; Lipson, M. Low-loss silicon platform for broadband mid-infrared photonics. *Optica* **2017**, *4*, 707.
(65) Yu, Y. F.; Zhu, A. Y.; Paniagua-Domínguez, R.; Fu, Y. H.; Luk'yanchuk, B.; Kuznetsov, A. I. High-transmission dielectric metasurface with 2π phase control at visible wavelengths. *Laser & Photonics Reviews* **2015**, *9*, 412−418.
(66) Hu, Y.; Luo, X.; Chen, Y.; Liu, Q.; Li, X.; Wang, Y.; Liu, N.; Duan, H. 3D-Integrated metasurfaces for full-colour holography. *Light: Sci. Appl.* **2019**, *8*, 86.

https://doi.org/10.1021/acs.nanolett.1c00356
Nano Lett. 2021, 21, 3849−3856